1

Plasmonic-Fluorescent and Magnetic-Fluorescent Composite Nanoparticle as Multifunctional Cellular Probe

Arindam Saha, SK Basiruddin, and Nikhil Ranjan Jana

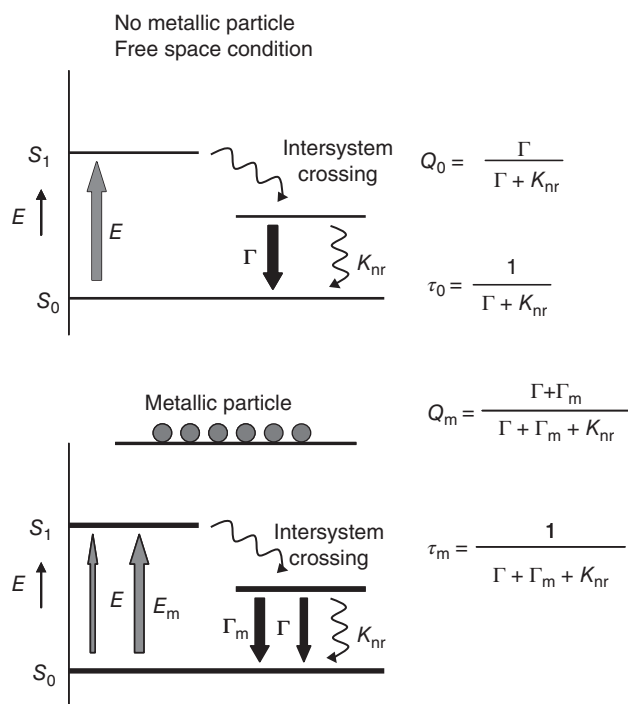*Centre for Advanced Materials, Indian Association for the Cultivation of Science, Kolkata, India*

1.1 Introduction

The interaction of fluorophore with metal has been a field of research since many decades. In 1970s, Drexhage found that fluorophore located near the metallic surfaces shows oscillations of the emissive lifetime depending on the distance from the metal surface [1, 2]. After this finding, many theoretical [3–9] and practical researches were directed in this field [10–16]. Now it is well known that when a metal surface interacts with an excited-state fluorophore, two phenomena can take place, either the fluorescence of the fluorophore is enhanced or it is quenched. When a metal stays very close to the fluorophore, typically within 20 nm, the electrons from the excited fluorophore transfer to the metal and hence result in fluorescence quenching. But when the metal surface stays 20–50 nm away from the fluorophore, the excited electrons of fluorophore interact differently with the metal electrons and it results in an increase in the rate of fluorescence decay as well as the rate of excitation. The effect is enhancement of fluorescence with decreased lifetime and increased photostability. This phenomenon is termed as metal-enhanced fluorescence (MEF) [14, 17, 18]. Most of this MEF has been observed for silver island film [17, 19–26], silver colloids [27–29], other silver nanostructures [30, 31], gold [32–35], iron oxide [36], tin [37], platinum [38], aluminium [39], and so on. Among different metals, nanosize silver and gold are studied more frequently as they have plasmonic properties in the visible region arising due to collective oscillations of surface electrons and that can significantly modulate the MEF properties.

Different options of a fluorophore under proper excitation are shown in Scheme 1.1. According to the aforementioned diagram, when a fluorophore is excited with an appropriate energy, it reaches to a higher electronic level and then undergoes decay in both radiative and non-radiative ways. Here Γ indicates the rate of radiative decay; K_{nr} is the rate of non-radiative decay and rate of quenching collectively. When the fluorophore is within the distance of 20 nm from the metal surface, then $K_{nr} > \Gamma$ and as a result both quantum yield (QY) (Q_0) and lifetime (τ_0) decrease. But when the distance between the metal surface and fluorophore is typically between 20 and 50 nm, $\Gamma > K_{nr}$ and hence Q_0 increases but τ_0 decreases, which is indicated by MEF. Since the lifetime decreases, the fluorophore remains in the excited state for a shorter time period and their chance of non-radiative decay or other excited state reaction is decreased that results in increased photostability [18, 23, 40–42]. When the distance is larger than 50 nm, there is preferably no interaction between the fluorophore and metal surface.

In fluorescence-based experiments (e.g., sensor application, cellular imaging, molecular probe design), metal-induced quenching is a critical drawback [43] and difficult to overcome completely. However, this quenching effect has been exploited as "Turn Off" detection of analyte in many cases, although this type of sensor design is neither specific nor accurate since many other factors can influence the quenching phenomenon. Alternative "Turn On" sensor design is of utmost importance where the presence of analyte is more selectively detected by the fluorescence enhancement effect [44]. In cellular imaging, the conventionally used molecular dyes often undergo photobleaching and hence long-term tracking of cellular activities is difficult. Although new dyes have been developed with reduced photobleaching properties, the quenching of the dye under complex cellular environment is unavoidable that often hinders the

No metallic particle
Free space condition

S_1

E

E

Intersystem crossing

Γ K_{nr}

S_0

$$Q_0 = \frac{\Gamma}{\Gamma + K_{nr}}$$

$$\tau_0 = \frac{1}{\Gamma + K_{nr}}$$

Metallic particle

$$Q_m = \frac{\Gamma + \Gamma_m}{\Gamma + \Gamma_m + K_{nr}}$$

S_1

E

E E_m

Intersystem crossing

Γ_m Γ K_{nr}

S_0

$$\tau_m = \frac{1}{\Gamma + \Gamma_m + K_{nr}}$$

Scheme 1.1 Different options of electron–hole recombination within a fluorophore. Here E and E_m are energy of excitation for fluorophore and metal plasmon.

imaging. Various semiconductors and other fluorescent nanoparticles are emerging as promising alternatives, but toxicity issues question their application potential for *in vivo* imaging and long-time cellular tracking [45–48].

The most adverse effect of metal-induced quenching occurs in the preparation of multifunctional probe, which is one of the current research directions. Various multifunctional probes composed of metallic and fluorescent components have been developed and many are still under development stages. These probes can be used for multiple applications like sensing, detection, imaging, and separation [49–55]. However, synthesis of these probes is a major challenge since the metal-based plasmonic or magnetic component in the composite system quenches the fluorescence of the fluorophore component. In order to solve this problem, various methods have been developed via tuning the separation distance between fluorescent components and quencher components, and in some selected cases MEFs are also observed [56–64].

We are interested in the development of noble metal nanoparticle-based hybrid nanoprobes composed of plasmonic and fluorescent components so that they can be used for different cellular labeling applications. Although noble metal nanoparticles have tunable optical property due to surface plasmon, their strong quenching property creates a difficulty in making hybrid nanoprobes. Thus appropriate methods need to be developed for synthesis, keeping optimum separation distance between the plasmonic and fluorescent components. In addition the methods should be simple and cost effective with options for various functionalizations. We have developed different methods to prepare different plasmonic-fluorescent nanoprobes that are composed of gold/silver nanoparticles of different sizes/shapes as plasmonic components and fluorescein or CdSe/ZnS quantum dots (QDs) as fluorescent components [65–68]. In addition to plasmonic-fluorescent hybrid nanoparticle, we are also developing magnetic metal oxide-based magnetic-fluorescent hybrid nanoparticles that can be used for magnetic separation applications [67, 68]. In all these hybrid nanoprobes, the fluorescence of the fluorophore component is partially quenched with the final QY ranging between 7 and 20%. These hybrid nanoparticles can be used for both fluorescence and plasmon-based imaging probes. Here we will summarize different approaches for their synthesis, functionalization, and application potential.

1.2 Synthesis Design of Composite Nanoparticle

Our research goal is to develop synthetic approach for plasmonic-fluorescent, magnetic-fluorescent, magnetic-plasmonic, or a combination of all the three components and applications of all these composites in various biomedical fields, such as cellular imaging, cellular

targeting and separation, protein detection, and study of carbohydrate–protein interaction. Here we will mainly focus on fluorescence-based composite materials. There are three general steps in the synthesis of these composite nanoparticles. First, high-quality hydrophobic nanoparticles, such as Au, Ag, CdSe/ZnS, and iron oxide; and hydrophilic nanoparticles, such as Au nanorod, Ag plate, Ag-coated Au nanorod have been synthesized by different reported methods [69–73]. Next, these as-synthesized nanoparticles are converted into polyacrylate-coated water-soluble nanoparticles when needed, using the reported methods [74–76]. Finally, composite materials have been synthesized using three different approaches shown in Scheme 1.2. Table 1.1 summarizes all types of composite nanoparticles prepared by these approaches along with their properties.

1.2.1 Method 1: Polyacrylate Coating-Based Composite of Nanoparticle and Organic Dye

This method can be employed for the preparation of plasmonic-fluorescent and magnetic-fluorescent composite nanoparticles between nanoparticle and organic dye [65, 66]. The preparation method is very similar to polyacrylate coating of nanoparticles with a modification where fluorescein methacrylate monomer is added along with other acrylate monomers so that fluorescein can be incorporated in the polyacrylate backbone. In this method IGEPAL cyclohexane-based reverse micelle solution has been used as a medium where hydrophobic nanoparticles and hydrophilic acryl monomers can be dissolved. The role of reverse micelle is to initiate the polyacrylate coating in homogeneous condition to minimize particle–particle aggregation during coating processes. The polymerization is initiated in the presence of an initiator ammonium persulfate under basic condition (N,N,N',N' tetramethylethylenediamine) and under inert atmosphere. The polymerization is stopped after 1 h by adding ethanol that precipitated the particles. The precipitated particles are washed with chloroform and ethanol and finally dissolved in fresh water. To further purify the composite system from free polymer, salt-induced precipitation and redispersion technique have been adapted followed by dialysis [65].

In the reaction condition, fluorescein methacrylate and other acryl monomers undergo simultaneous polymerization and are coated on the nanoparticle surface making 5–10 nm shells. Since the polymerization is random, fluorescein molecules are attached randomly on the polymeric coating backbone making a distance distribution between fluorescein and core nanoparticle. Different polymers forming acryl monomer can be used to provide different chemical functional groups on the coating backbone and on the nanoparticle surface. For example, N-(3-aminopropyl)methacrylamide hydrochloride has been used to provide primary amine functionality, acrylic acid for carboxylate functionality, poly(ethylene glycol) methacrylate for polyethylene glycol functionality, and methylene *bis*acrylamide is used to crosslink the polymer for a robust coating.

1.2.2 Method 2: Polyacrylate Coating-Based Composite of Two Different Nanoparticles

This method is useful for the synthesis of magnetic-fluorescent and plasmonic-fluorescent composite nanoparticles using two different nanoparticle components [67]. Here inorganic semiconductor nanoparticles are employed as fluorescent components and metal or metal oxides are used as plasmonic or magnetic components. The semiconductor nanoparticles of CdSe with ZnS shell QD have been prepared in different sizes ranging from 2 to 6 nm using the colloidal chemical synthesis method reported earlier [69]. These semiconductor nanoparticles have sizes less than the excitonic Bohr radius showing the quantum confinement effect and the bandgap between valence band and conduction band can be tuned by changing the particle size. The smaller the size higher the bandgap and hence the emission maxima blueshifted. Hence by tuning the size, we can have nanoparticles of various emissions (e.g., red, yellow, green). Other component nanoparticles such as gold, silver, and iron oxide in the size range of 5–50 nm have been prepared using standard methods. All the as-synthesized nanoparticles are purified from free surfactants and dispersed in solvents prior to their use.

Composite nanoparticle synthesis approach is very similar to polyacrylate coating method described in Method 1, except that two nanoparticles are used during polyacrylate coating. In this method both the nanoparticles are taken in reverse micelle along with polymer-forming monomer precursors, and polymerization is performed in that condition so that both nanoparticles are encapsulated inside a common polymeric shell. Since the reverse micelle is a dynamic assembly, the polymerization process can randomly trap different nanoparticles inside a single polymeric shell with the formation of a composite nanoparticle. The composition of composite can be controlled by varying the concentration ratio of the two nanoparticles. The polymer shell structure and functionality can be controlled by using different polymer precursors. Adjusting the polymerization condition composite
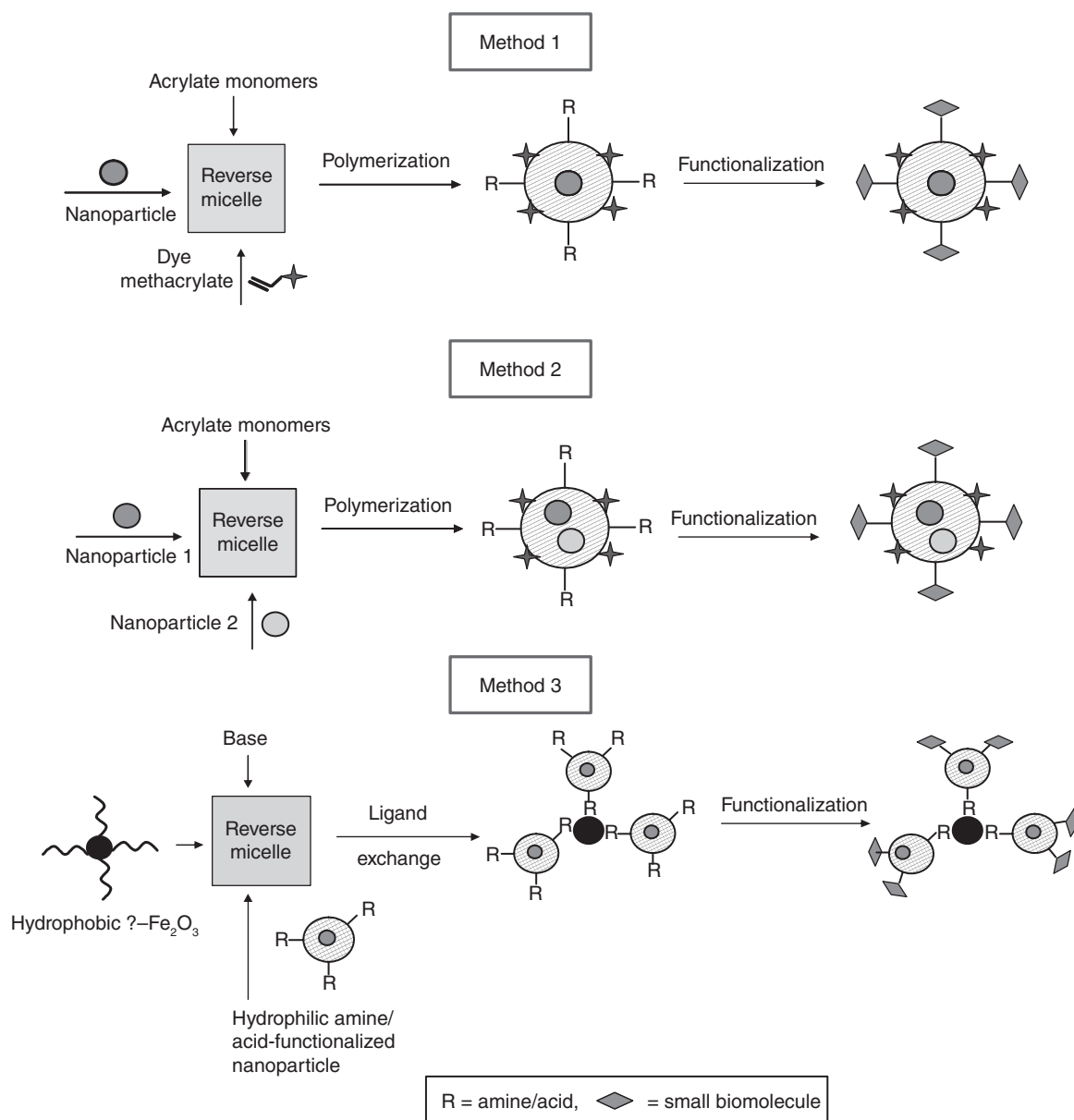
Scheme 1.2 Different synthesis approaches for multifunctional nanoparticle.

nanoparticle can be prepared having good water solubility and with 8–20% fluorescence QY. These composite nanoparticles can be purified by methods described in Method 1.

1.2.3 Method 3: Ligand Exchange Approach-Based Composite of Two Different Nanoparticles

This method is useful for the preparation of magnetic-fluorescent and magnetic-plasmonic nanocomposites, and here we will discuss only magnetic-fluorescent

nanocomposites [68]. The ligand exchange approach is well known for the conversion of hydrophobic nanoparticle into hydrophilic nanoparticle. In this method, a thiol-based hydrophilic molecule is mixed with hydrophobic surfactant-capped gold or QD nanoparticle. As thiols have strong interaction with Au or Zn surface, they adsorb on the nanoparticle surface by replacing hydrophobic surfactants, making water-soluble nanoparticles. Thus conventional ligand exchange involves exchange of ligands on a nanoparticle surface. Here we have extended the ligand exchange approach involving two nanoparticles where ligands present on

Table 1.1 Summary of different composite nanoparticles along with their properties and application potentials.

Composite composition	Composite property	Preparation method	Overall size (nm)	Quantum yield (%)	Application
Au–fluorescein	Plasmonic and fluorescent	Method 1	20–40	16	Dual imaging (fluorescence and dark field), protein detection
Ag–fluorescein	Plasmonic and fluorescent	Method 1	20–40	12	Dual imaging (fluorescence and dark field), protein detection, antibacterial activity
Au nanorod–fluorescein	Plasmonic and fluorescent	Method 1	<100	9	Dual imaging (fluorescence and dark field), protein detection, photothermal therapy
Ag-coated Au nanorod–fluorescein	Plasmonic and fluorescent	Method 1	~65	8	Dual imaging (fluorescence and dark field), SERS[a]-based detection
γ-Fe$_2$O$_3$–fluorescein	Magnetic and fluorescent	Method 1	20–40	20	Fluorescence imaging, magnetic separation, MRI
γ-Fe$_2$O$_3$-CdSe/ZnS	Magnetic and fluorescent	Methods 2 and 3	50–80 (Method 2)	8–20	Fluorescence imaging, magnetic separation, MRI
			20–30 (Method 3)		

[a] SERS, surface-enhanced Raman scattering.

the surface of one nanoparticle replace the ligand present on another nanoparticle surface. Specifically we have mixed two types of nanoparticles, one coated with hydrophobic ligands and the other coated with hydrophilic ligands. The hydrophilic coating is exposed with surface chemical functionality that has strong affinity to other nanoparticle and thus replaces the hydrophobic ligands of the other nanoparticle. These processes lead to the formation of a composite nanoparticle.

We have used surfactant-coated hydrophobic iron oxide nanoparticle and polyacrylate-coated hydrophilic QD for this work. Polyacrylate-coated QDs are synthesized using the technique mentioned previously. This coating provides surface amine/acid group on QD nanoparticle surface. In contrast hydrophobic iron oxide nanoparticle has a long-chain fatty acid/amine capping. For the ligand exchange, the hydrophobic iron oxide is first dissolved in reverse micelle and then hydrophilic QDs are added under basic condition. At this condition long-chain fatty acid/amine capping on iron oxide surface is replaced by the surface amine/acid of polyacrylate-coated QDs. Next, ethanol is added to precipitate the hybrid material. The supernatant is decanted, and the precipitate has been washed repeatedly with cyclohexane and chloroform. This washing step removes any free hydrophobic γ-Fe$_2$O$_3$ as they are soluble in cyclohexane and chloroform. During each washing step, the hybrid materials are magnetically separated from the solution. This magnetic separation removes any free hydrophilic nanoparticle from the hybrid particle. After these washing steps, the hybrid

materials have been dried in air and finally dissolved in water or a buffer solution.

The success of this process depends on the type of long-chain ligand on iron oxide surface and the type of surface functional group on QDs. Proper adjustment of these two factors results in efficient ligand exchange to produce magnetic-fluorescent composite nanoparticles. It is also possible to control the number of QDs on the iron oxide surface by adjusting the ratio of two nanoparticle concentrations and by controlling the amine/acid on the polyacrylate backbone of QDs. The fluorescence QY of the composites depends on the amount of QD over each iron oxide nanoparticle surface and typically varies from 8 to 20%. Composite nanoparticle produced by this approach can be further functionalized using the primary amine/carboxylate present on the QD surface.

1.3 Property of Composite Nanoparticles

1.3.1 Optical Property

We have prepared plasmonic-fluorescent (Au, Ag, Au nanorod, and Ag plate as plasmonic component) and magnetic-fluorescent (γ-Fe$_2$O$_3$ and Fe$_3$O$_4$ as magnetic component) composite materials using the aforementioned three different approaches (Table 1.1). All these hybrid nanoparticles are water soluble with good colloidal stability in various buffer media. Figure 1.1 shows
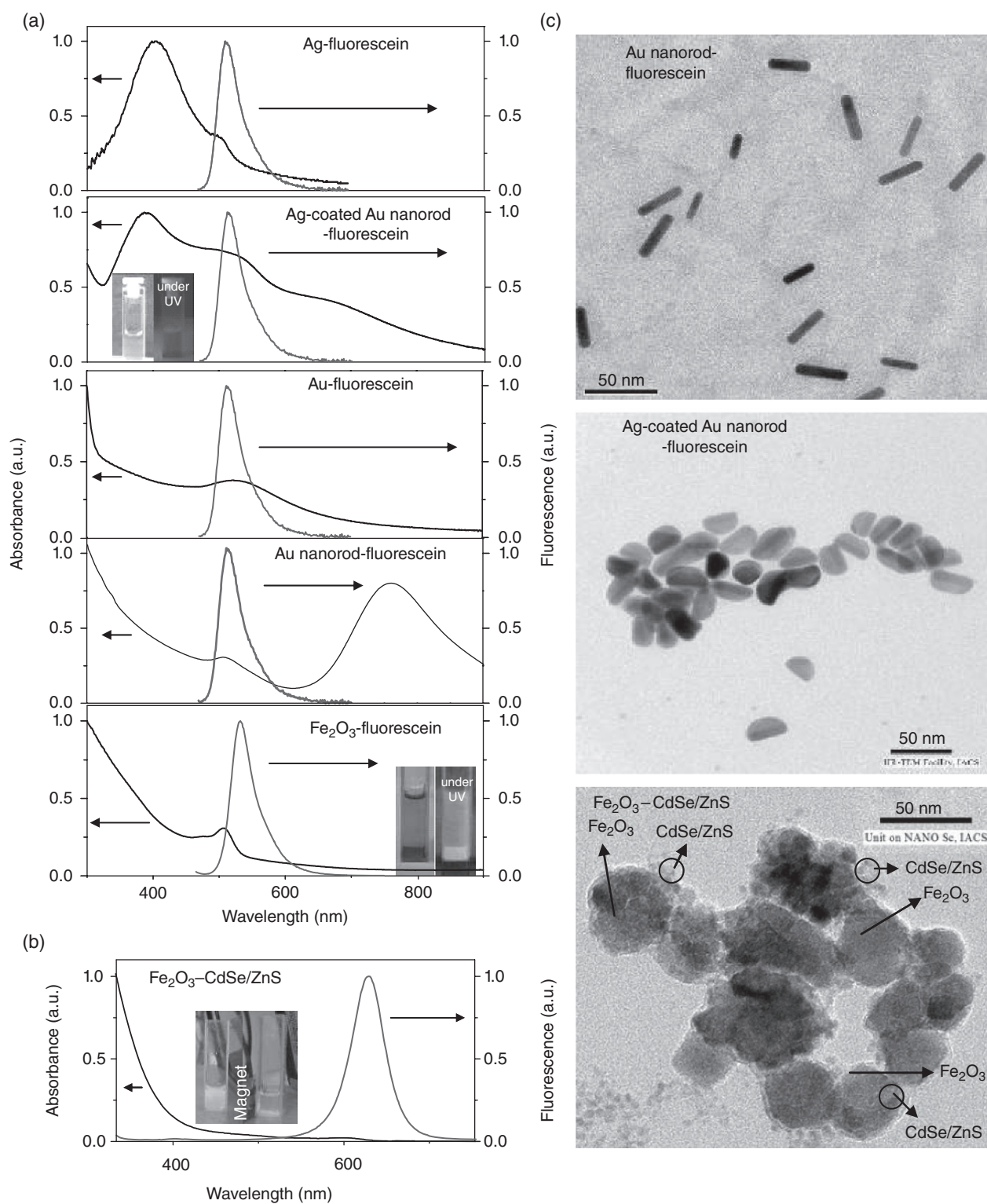
(a)

(b)

(c)

Figure 1.1 UV–Vis and fluorescence spectra of fluorescein-based composite nanomaterials (inset digital images of plasmonic-fluorescent and magnetic-fluorescent composites along with normal light and UV light and/or magnetic separation under UV light) (a), UV–Vis and fluorescence spectra of QD-based composite nanomaterials (b), and TEM image of Au nanorod–fluorescein, Ag-coated Au nanorod–fluorescein, and γ-Fe$_2$O$_3$–CdSe/ZnS composite (c).

representative ultraviolet (UV)–visible (Vis) and photoluminescence spectra of different plasmonic-fluorescent and magnetic-fluorescent nanoparticles showing plasmonic-fluorescent and magnetic-fluorescent properties (Figure 1.1). In the UV–Vis spectra of Au–fluorescein, the peak at around 530 nm is due to plasmonic property of Au nanoparticles, and the peak around 510 nm is due to the absorbance of fluorescein. Due to this fluorescein absorption, the plasmonic peak of Au becomes broad. In the case of Ag-fluorescein, two peaks are observed in the UV–Vis spectra—510 nm peak corresponds to fluorescein absorption, and 410 nm peak corresponds to plasmonic absorption of Ag nanoparticles. In Au nanorod–fluorescein, two peaks of Au nanorod are observed at 520 and 800 nm, which are due to transverse and longitudinal oscillation of plasmonic electrons along the nanorod's short and long axes, respectively. But the peak at 520 nm broadens due to fluorescein absorption. The Ag-coated Au nanorod–fluorescein composites show three distinct humps corresponding to plasmonic peaks of Ag and Au in 400–800 nm regions. In case of iron oxide-fluorescein only, the fluorescein absorption peak is observed since iron oxide does not have any absorption in the visible region. In all these plasmonic-fluorescent composite nanoparticles, the photoluminescence spectra show the characteristic green emission of fluorescein with a peak at around 528 nm. The digital images show plasmonic color under normal light and characteristic green emission under UV light irradiation. The QY of these composite nanoparticles is calculated using fluorescein as a standard (95% QY). The concentration of fluorescein is calculated from the absorption spectra of hybrid nanoparticles in both acidic and basic pH. Fluorescein shows no absorption at 500 nm in acidic pH but shows significant absorption in basic pH, and this fact has been used to calculate the fluorescein concentration. Fluorescence QY is calculated as 12% for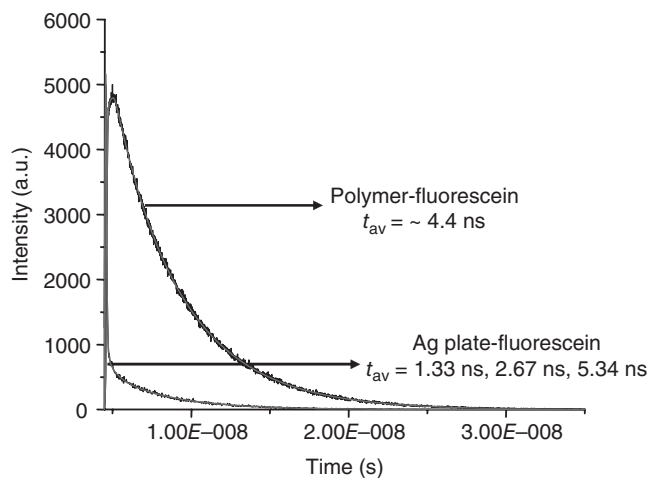 Ag– fluorescein, 16% for Au–fluorescein, 9% for Au nanorod–fluorescein, 8% for Ag-coated Au nanorod–fluorescein, and ~20% for iron oxide–fluorescein.

Semiconductor nanoparticle QD-based composites (iron oxide QD and Au nanorod QD) show fluorescent properties characteristic of semiconductor nanoparticle. In Figure 1.1b UV–Vis spectrum and photoluminescence property of such particles have been shown. In the UV–Vis spectrum, a small hump at 600 nm corresponds to QD's first excitonic peak, which arises due to the transition of electrons from the highest energy level of valence band to the lowest energy level of conduction band. When these composites are excited using 350 nm light, it produces sharp emission spectra centered around 630 nm, which arises due to electron–hole recombination. Magnetic property of these composites can be realized from the digital image showing magnetic separation of these particles under magnet once their colloidal stability is lowered by adding salt. These composite nanoparticles also show fluorescence QY in the range of 8–20%, depending on the size of QD used.

1.3.2 Fluorophore Lifetime Study

The fluorescence QY data suggests that fluorophores in composite nanoparticle are distributed around metal/metal oxide keeping a separation distance so that the fluorescence is not completely quenched. In order to understand in more detail the nature of interaction between fluorophore and metal/metal oxide, we performed lifetime measurements of fluorophore in the composite nanoparticle. Figure 1.2 shows a representative result of the lifetime study. Analyzing the fluorescent lifetime data of the plasmonic-fluorescent nanocomposites, we have found that lifetime decreases and decay curve fits with the multiple exponential, compared to single exponential fitting for fluorescein. For example, fluorescein itself has an average lifetime of ~4.4 ns, but in composites

Figure 1.2 Lifetime data for polymer fluorescein that is best fitted in a single exponential curve and for Ag plate–fluorescein composite that best fitted in three exponential curves with decreased lifetime. Dotted line corresponds to experimental data and bold line corresponds to fitting curve.

the decay curve best fits with three exponentials with the decrease in average lifetime. In case of Ag–fluorescein, the average lifetimes are 0.46, 2.43, and 4.12 ns; for Au–fluorescein, they are 0.05, 0.88, and 3.47 ns; for Au nanorod–fluorescein, the values are 0.2, 1.8, and 3.6 ns; and for Ag plate–fluorescein, the values are 1.33, 2.67, and 5.34 ns. Lowering of average lifetime and decrease in fluorescence QY in all these samples suggest a significant quenching effect of fluorophore fluorescence. Three different lifetimes suggest that the fluorophores are at various distances from the plasmonic nanoparticles and greater the distance from the core, the higher the average lifetime is. This distance-dependent distribution of fluorophore results in the partial quenching effect. Similar type of lifetime data has also been observed in case of other QD-based composite nanoparticles suggesting that the behavior of fluorescent dye or fluorescent nanoparticle (QDs) in composite nanoparticles is similar. Nevertheless, the final composite contains sufficient fluorescence for multifunctional application.

1.4 Functionalization and Labeling Application of Composite Nanoparticle

The composite nanomaterials prepared by various methods are water soluble with the scope for further functionalization. In TEM study of fluorescein-based composite nanoparticle, the core nanoparticles can be visualized but the fluorescein-incorporated polyacrylate shell is invisible unless proper staining is performed (Figure 1.1c). Similarly, for two nanoparticle-based composites, both nanoparticles can be detected in TEM but not their polymer shells (Figure 1.1c). DLS study offers the hydrodynamic diameter of these composite nanomaterials including the polymer shells and the overall size ranges between 20 and 80 nm (Table 1.1). These composite nanoparticles have been functionalized with various biomolecules such as glucose, oleyl, vancomycin, TAT peptide, and so on. Standard conjugation chemistries like glutaraldehyde-based coupling, *N*-succinimidyl 4-(maleimidomethyl)cyclohexane-carboxylate (SMCC)-based conjugation, and 1-ethyl-3-(3-dimethylaminopropyl)carbodiimide (EDC) coupling [68, 74] have been applied for covalent conjugation with a nanoparticle. In most of these works, the primary amine functional groups present on the composite nanoparticle surface have been used for conjugation chemistry.

These composite nanoparticles have potential multifunctional applications. For example, a plasmonic-fluorescent nanoparticle can be used as a dual imaging probe such as fluorescence imaging using fluorescent component and scattering-based dark field imaging using a plasmonic component or imaging and detection probe such as fluorescence-based imaging and plasmon-based detection [65, 66]. The magnetic-fluorescent nanoparticle can be used for fluorescence-based imaging and magnetic separation [67, 68]. We have used functionalized composite nanoparticles for multifunctional cellular imaging and cell separation applications. Oleyl functionalization offers cell membrane targeting, TAT functionalization offers increased cellular internalization, and glucose or vancomycin functionalization offers specific cell targeting and labeling [65–68]. When imaged under fluorescence microscope, labelled cells show bright fluorescence due to fluorophore components, and both fluorescein dye and QD are photostable for long-term cellular imaging [65, 67]. Similarly, the dark field imaging shows bright colors of labeled cells due to plasmonic components (Figure 1.3). Magnetic separation of labeled cells has also been studied when magnetic component is present in the composite nanoparticle. We have also extended this work for bacteria imaging and separation using vancomycin-functionalized magnetic-fluorescent composites [67] (Figure 1.3).

Specific detection of protein has been performed using glucose-functionalized nanocomposites via specific interaction with glycoprotein concanavalin A (Con A). Con A has four binding sites for glucose, which upon interaction with glucose crosslink the particles and causes precipitation of particles from the solution [66]. The glucose-functionalized Au nanorod–fluorescein composite responds to a very small change in Con A concentration, since the longitudinal peak of Au nanorod is very sensitive to aggregation. This probe can be extended for imaging of glycoprotein in cellular environment or magnetic separation of glycoprotein from extracellular environment. These examples show that the composite nanoparticle can be used for a variety of multifunctional applications such as optical detection and imaging or separation.

1.5 Conclusion

Metal-induced fluorescence quenching is a major drawback in numerous fluorescence-based applications, particularly in multifunctional composite probe design. In contrast, MEF, which can be observed for an optimum distance between fluorophore and metal, has a great potential in overcoming this quenching problem.
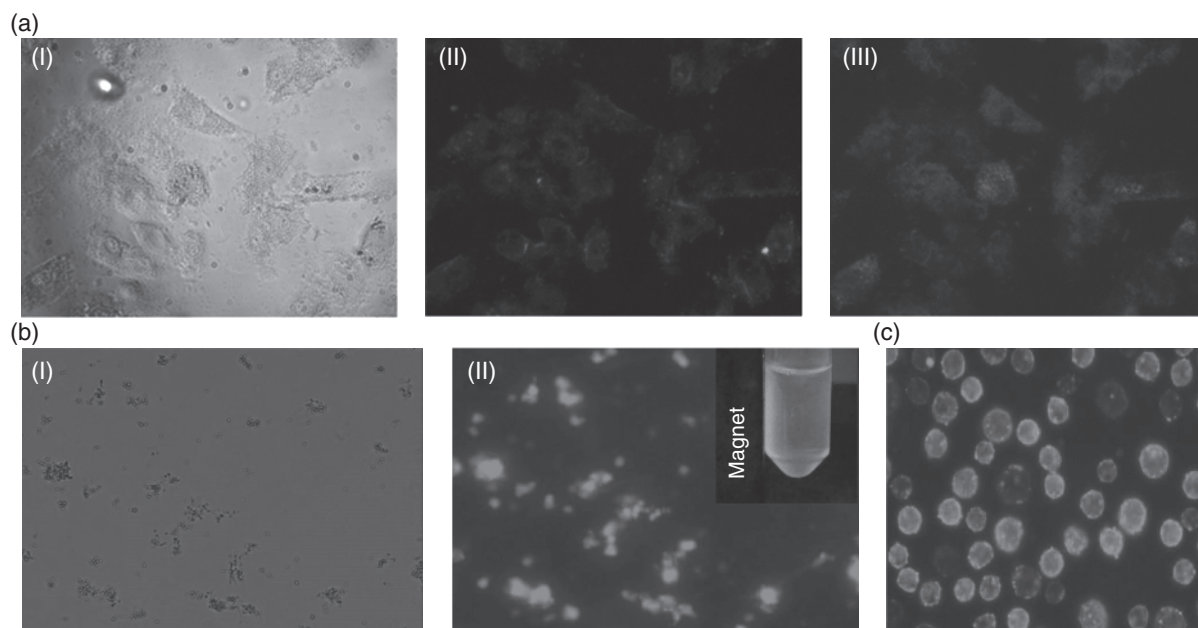
Figure 1.3 (a) H9C2 cells treated with oleyl-functionalized Au nanorod–fluorescein composite. (I) Bright field image, (II) fluorescence image, and (III) dark field image. (b) *Bacillus subtilis* bacteria treated with vancomycin-functionalized γ-Fe$_2$O$_3$–CdSe/ZnS nanocomposite (I) bright field image and (II) fluorescence image (inset magnetic separation of bacteria). (c) Fluorescence image of EAC cell treated with oleyl-functionalized γ-Fe$_2$O$_3$–CdSe/ZnS nanocomposite. (*See insert for color representation of this figure.*)

However, very limited success has been achieved in this direction due to the difficulty in controlling the distance between fluorophore and metal. We have designed three different strategies for the synthesis of multifunctional composite nanoparticles that overcome the quenching problem completely. The designs are such that fluorophores are distributed at various distances from the core metallic particle and only partial quenching of the fluorophores is observed in average. The resultant composite nanoparticle can be used as multifunctional probes for different biomedical applications. We have applied these probes for dual imaging, imaging-separation, and detection-separation applications.

Acknowledgments

References

1 Drexhage, K. H. *J. Lumin.* **1970**, *12*, 693.

2 Drexhage, K. H. *Progress in Optics, Vol. XII*; Wolf, E., Ed.; North Holland Publishing Company: Amsterdam, **1974**.

3 Tews, K. H. *J. Lumin.* **1974**, *9*, 223.

4 Chance, R. R.; Prock, A.; Silbey, R. *J. Chem. Phys.* **1974**, *60*, 2744.

5 Persson, B. N. J. *J. Phys. C, Solid State Phys.* **1978**, *11*, 4251.

6 Gersten, J.; Nitzan, A. *J. Chem. Phys.* **1981**, *75*, 1139.

7 Ruppin, R. *J. Chem. Phys.* **1982**, *76*, 1681.

8 Barnes, W. L. *J. Mod. Opt.* **1998**, *45*, 661.

9 Das, P. C.; Puri, A. *Phys. Rev. B* **2002**, *65*, 155416/1.

10 Adams, A.; Rendell, R. W.; Garnett, R. W.; Hansma, P. K.; Metiu, H. *Opt. Commun.* **1980**, *34*, 417.

11 Weitz, D. A.; Garoff, S.; Hanson, C. D.; Gramila, T. *J. Opt. Lett.* **1982**, *7*, 89.

12 Leitner, A.; Lippitsch, M. E.; Draxler, S.; Riegler, M.; Aussenegg, F. R. *Appl. Phys. B* **1985**, *36*, 105.

13 Aussenegg, F. R.; Leitner, A.; Lippitsch, M. E.; Reinisch, H.; Riegler, M. *Surf. Sci.* **1987**, *139*, 935.

14 Sokolov, K.; Chumanov, G.; Cotton, T. M. *Anal. Chem.* **1998**, *70*, 3898.

15 Tarcha, P. J.; De Saja-Gonzalez, J.; Rodriguez-Llorente, S.; Aroca, R. *Appl. Spectrosc.* **1999**, *53*, 43.

16 De Saja-Gonzalez, J.; Aroca, R.; Nagao, Y.; De Saja, J. A. *Spectrochim. Acta A* **1997**, *53*, 173.

17 Lakowicz, J. R. *Anal. Biochem.* **2001**, *298*, 1.

18 Geddes, C. D.; Lakowicz, J. R. *J. Fluores.* **2002**, *12*, 121.

19 Lakowicz, J. R.; Shen, Y.; D'Auria, S.; Malicka, J.; Fang, J.; Gryczynski, Z.; Gryczynski, I. *Anal. Biochem.* **2002**, *301*, 261.

20 Gryczynski, I.; Malicka, J.; Holder, E.; DiCesare, N.; Lakowicz, J. R. *Chem. Phys. Lett.* **2002**, *372*, 409.

21 Lakowicz, J. R.; Maliwal, B. P.; Malicka, J.; Gryczynski, Z.; Gryczynski, I. *J. Fluoresc.* **2002**, *12*, 431.

22 Gryczynski, I.; Malicka, J.; Shen, Y.; Gryczynski, Z.; Lakowicz, J. R. *J. Phys. Chem. B* **2002**, *106*, 2191.

23 Malicka, J.; Gryczynski, I.; Gryczynski, Z.; Lakowicz, J. R. *Anal. Biochem.* **2003**, *315*, 57.

24 Lakowicz, J. R.; Malicka, J.; D'Auria, S.; Gryczynski, I. *Anal. Biochem.* **2003**, *320*, 13.

25 Malicka, J.; Gryczynski, I.; Lakowicz, J. R. *Anal. Chem.* **2003**, *75*, 4408.

26 Malicka, J.; Gryczynski, I.; Maliwal, B. P.; Fang, J.; Lakowicz, J. R. *Biopolymers* **2003**, *72*, 96.

27 Maliwal, B. P.; Malicka, J.; Gryczynski, I.; Gryczynski, Z.; Lakowicz, J. R. *Biopolymers* **2003**, *70*, 585.

28 Geddes, C. D.; Cao, H.; Gryczynski, I.; Gryczynski, Z.; Fang, J.; Lakowicz, J. R. *J. Phys. Chem. A* **2003**, *107*,3443.

29 Lukomska, J.; Malicka, J.; Gryczynski, I.; Lakowicz, J. R. *J. Fluoresc.* **2004**, *14*, 417.

30 Parfenov, A.; Gryczynski, I.; Malicka, J.; Geddes, C. D.; Lakowicz, J. R. *J. Phys. Chem. B* **2003**, *107*, 8829.

31 Geddes, C. D.; Parfenov, A.; Lakowicz, J. R. *Appl. Spectrosc.* **2003**, *57*, 526.

32 Pompa, P. P.; Martiradonna, L.; Della Torre, A.; Della Sala, F.; Manna, L.; De Vittorio, M.; Calabi, F.; Cingolani, R.; Rinaldi, R. *Nature Nanotechnol.* **2006**, *1*, 126.

33 Zhang, J.; Lakowicz, J. R. Opt. Express **2006**, *15*, 2598.

34 Fu, Y.; Zhang, J.; Lakowicz, J. R. *J. Am. Chem. Soc.* **2010**, *132*, 5540.

35 Hwang, A.; Smolyaninov, I. I.; Davis, C. C. *Nano Lett.*, **2010**, *10*, 813.

36 Zhang, Y.; Padhyay, A.; Sevilleja, J. E.; Guerrant, R. L.; Geddes, C. D. *J. Phys. Chem. C* **2010**, *114*, 7575.

37 Zhang, Y.; Dragan, A.; Geddes, C. D. *J. Appl. Phys.* **2010**, *107*, 024302.

38 Ray, K.; Chowdhury, M. H.; Lakowicz, J. R. *Chem. Phys. Lett.* **2008**, *465*, 92.

39 Chowdhury, M. H.; Ray, K.; Gray, S. K.; Pond, J.; Lakowicz, J. R. Proceedings of SPIE—the International Society for Optical Engineering, **2010**, *7577*, 75770O.

40 Ray, K.; Szmacinski, H.; Enderlein, J.; Lakowicz, J. R. *Appl. Phys. Lett.* **2007**, *90*, 251116.

41 Gryczynski, I.; Malicka, J.; Nowaczyk, K.; Gryczynski, Z.; Lakowicz, J. R. *J. Phys. Chem. B* **2004**, *108*, 12073.

42 Fu, Y.; Lakowicz, J. R. *Laser Photon. Rev.* **2009**, *3*, 221.

43 Zhang, J.; Badugu, R.; Lakowicz, J. R. *Plasmonics*, **2007**, *3*, 3.

44 Tan, S. S.; Kim, S. J.; Kool, E. T. *J. Am. Chem. Soc.* **2011**, *133*, 2664.

45 Hoshino, A.; Fujioka, K.; Oku, T.; Suga, M.; Sasaki, Y. F.; Ohta, T.; Yasuhara, M.; Suzuki, K.; Yamamoto, K. *Nano Lett.* **2004**, *4*, 2163.

46 Derfus, A. M.; Chan, W. C. W.; Bhatia, S. N. *Nano Lett.* **2004**, *4*, 11.

47 Kirchner, C.; Liedl, T.; Kudera, S.; Pellegrino, T.; Javier, A. M.; Gaub, H. E.; Stoelzle, S.; Fertig, N.; Parak, W. *J. Nano Lett.* **2005**, *5*, 331.

48 Bentzen, E. L.; Tomlinson, I. D.; Mason, J.; Gresch, P.; Warnement, M. R.; D. Wright, D.; Sanders-Bush, E.; Blakely, R.; Rosenthal, S. *J. Bioconjugate Chem.* **2005**, *16*, 1488.

49 Wang, D.; He, J.; Rosenzweig, N.; Rosenzweig, Z. *Nano Lett.* **2004**, *4*, 409.

50 Sathe, T. R.; Agrawal, A.; Nie, S. *Anal. Chem.* **2006**, *78*, 5627.

51 Selvan, S. T.; Patra, P. K.; Ang, C. Y.; Ying, J. Y. *Angew Chem. Int. Ed.* **2007**, *46*, 2448.

52 Park, J.-H.; von Maltzahn, G.; Ruoslahti, E.; Bhatia, S. N.; Sailor, J. M. *Angew Chem. Int. Ed.* **2008**, *47*, 7284.

53 Kim, J.; Kim, H. S.; Lee, N.; Kim, T.; Kim, H.; Yu, T.; Song, I. C.; Moon, W. K.; Hyeon, T. *Angew Chem. Int. Ed.* **2008**, *47*, 8438.

54 Stoeva, S. I.; Lee, J.-S.; Smith, J. E.; Rosen, S. T.; Mirkin, C. A. *J. Am. Chem. Soc.* **2006**, *128*, 8378.

55 Gole, A.; Agarwal, N.; Nagaria, P.; Wyatt, M. D.; Murphy, C. *J. Chem. Commun.* **2008**, *46*, 6140.

56 Zhang, J.; Fu, Y.; Li, G.; Nowaczyk, K.; Zhao, R. Y.; Lakowicz, J. R. *Biochem. Biophys. Res. Commun.* **2010**, *400*, 111.

57 Lakowicz, J. R.; Malicka, J.; Gryczynski, I.; Gryczynski, Z. *Biochem. Biophys. Res. Commun.* **2003**, *307*, 435.

58 Badugu, R.; Lakowicz, J. R.; Geddes, C. D. *J. Am. Chem. Soc.* **2005**, *127*, 3635.

59 Zhang, J.; Fu, Y.; Liang, D.; Zhao, R. Y.; Lakowicz, J. R. *Langmuir* **2008**, *24*, 12452.

60 Aslan, K.; Wu, M.; Lakowicz, J. R.; Geddes, C. D. *J. Am. Chem. Soc.* **2007**, *129*, 1524.

61 Malicka, J.; Gryczynski, I.; Geddes, C. D.; Lakowicz, J. R. *J. Biomed. Opt.* **2003**, *8*, 472.

62 Aslan, K.; Lakowicz, J. R.; Szmacinski, H.; Geddes, C. D. *J. Fluores.*, **2004**, *1*, 677.

63 Aslan, K.; Huang, J.; Wilson, G. M.; Geddes, C. D. *J. Am. Chem. Soc.* **2006**, *128*, 4206.

64 Zhang, J.; Fu, Y.; Liang, D.; Nowaczyk, K.; Zhao, R. Y.; Lakowicz, J. R. *Nano Lett.*, **2008**, *8*, 1179.

65 Saha, A.; Basiruddin, SK.; Sarkar, R.; Pradhan, N.; Jana, N. R. *J. Phys. Chem. C* **2009**, *113*, 18492.

66 Basiruddin, SK.; Saha, A.; Pradhan, N.; Jana, N. R. *Langmuir* **2010**, *26*, 7475.

67 Basiruddin, SK.; Saha, A.; Sarkar, R.; Majumder, M.; Jana, N. R. *Nanoscale*, **2010**, *2*, 2561.

68 Saha, A.; Basiruddin, SK.; Pradhan, N.; Jana, N. R. *Langmuir* **2010**, *26*, 4351.

69 Li, J. J.; Wang, Y. A.; Guo, W.; Keay, J. C.; Mishima, T. D.; Johnson, M. B.; Peng, X. *J. Am. Chem. Soc.* **2003**, *125*, 12567.

70 Jana, N. R.; Peng, X. *J. Am. Chem. Soc.* **2003**, *125*, 14280.

71 Jana, N. R.; Chen, Y.; Peng, X. *Chem. Mater.* **2004**, *16*, 3931.

72 Jana, N. R. *Small* **2005**, *1*, 875.

73 Jiang, J.; Gu, H.; Shao, H.; Devlin, E.; Papaefthymiou, G. C.; Ying, J. Y. *Adv. Mater.* **2008**, *20*, 4403.

74 Wei, Y.; Jana, N. R.; Tan, S.; Ying, J. Y. *Bioconjugate Chem.* **2009**, *20*, 1752.

75 Tan, S. J.; Jana, N. R.; Gao, S.; Patra, P. K.; Ying, J. Y. *Chem. Mater.* **2010**, *22*, 2239.

76 Basiruddin, SK.; Saha, A.; Pradhan N.; Jana, N. R. *J. Phys. Chem. C*, **2010**, *114*, 11009.